



Boosting photocatalytic performance and stability of CuInS₂/ZnS-TiO₂ heterostructures via sol-gel processed integrate amorphous titania gel

Long Kong, Zhichun Li, Shouqiang Huang, Jinping Jia, Liang Li*

School of Environmental Science and Engineering, Shanghai Jiao Tong University, 800 Dongchuan Road, Shanghai 200240, PR China



ARTICLE INFO

Article history:

Received 16 September 2016

Received in revised form

22 November 2016

Accepted 24 November 2016

Available online 25 November 2016

Keywords:

Photocatalysis

Amorphous TiO₂ coatings

CIS/ZnS-TiO₂ gel

Photocorrosion

Cr (VI) reduction

ABSTRACT

Semiconductor quantum dots (QDs) are interesting photocatalysts for solar fuel production and environmental pollution control. However, the poor stability and recombination probability of photogenerated electron-hole pairs prevented the practical applications of QDs based photocatalysts. Herein we demonstrated that the incorporation of amorphous titania (TiO₂) coatings with CuInS₂/ZnS-TiO₂ heterostructures (CIS/ZnS-TiO₂ gel) can markedly boost photocatalytic performance and stability for Cr (VI) reduction. The promoted photocatalytic activity of CIS/ZnS-TiO₂ gel is associated with the enhanced light-absorption and distinctive heterojunction imposed by the integration of CIS/ZnS-TiO₂ with amorphous TiO₂ coatings, which drastically speed the separation of photogenerated electron-hole pairs. Moreover, the physical protection and photocorrosion-inhibition functions (receptors of photogenerated holes from CIS/ZnS QDs) arised from the amorphous TiO₂ coatings were mainly responsible for the promoted photo-stability of CIS/ZnS-TiO₂ gel. Our CIS/ZnS-TiO₂ gel retained over 90% of its initial activity under cycle tests, while the bared CIS/ZnS-TiO₂ showed a distinct reduction (approximately 35%) of its original efficiency due to the photocorrosion and weight-loss. Obviously, the incorporation of amorphous TiO₂ along with its bulk appearance of gel realized the enhanced photocatalytic performance with a favorable cycling stability. This strategy could be extended to other QDs-based photocatalysts in improving photocatalytic performance toward practical application.

© 2016 Elsevier B.V. All rights reserved.

1. Introduction

With an increasing attention toward water purification and energy conversion problems, photocatalysis have been extensively utilized to settle these issues owing to its efficient and eco-friendly features [1,2]. Semiconductor quantum dots (QDs), with narrow band gaps, high absorption coefficient, easy adjustability of optic and electronic properties, have worked as promising candidates for solar light-driven photocatalysts [3–5]. Heterojunction structures combined QDs with other semiconductors, notably TiO₂, have been developed as an effective strategy to overcome the rapid recombination of photogenerated electron-hole pairs of QDs which restricted their photocatalytic performance [6]. For instance, TiO₂/CdSe [7], TiO₂/CdS [3,5], TiO₂/PbSe [8], TiO₂/PbS [9], and TiO₂/CuInS₂ [10] were widely investigated. CuInS₂ QDs, environment-friendly with relatively biocompatible composition, are considered as a promising alternate to Cd and Pb based QDs [10,11].

Unfortunately, QDs (e.g. CuInS₂ QDs) as the photocatalysts exhibited inherent drawback of poor stability resulted from the surrounding environment inducing surface oxidation and photocorrosion by excess photogenerated holes under long term light irradiation [12]. Therefore, it is a key issue to enhance the stability of QDs and increase the recyclability of the corresponding heterojunction photocatalyst. The traditional silica coatings have been widely studied to barrier QDs from oxygen and consequently and improve the stability of QDs [13,14]. Meanwhile, silica coatings might block the transport of the photogenerated electrons and holes on the interfaces of semiconductors. Similarly, as proved in our previous studies, Al₂O₃ self-passivation layer drastically improved the stability of CuInS₂ QDs and Cd based QDs [15,16]. Whereas, the Al₂O₃ layer hampered the transfer of electrons and resulted in a decreased photocatalytic activity in our CuInS₂/ZnS:Al-TiO₂ photocatalyst [17], which was also observed in a dye-sensitized TiO₂ system [18]. Thus, when it comes to photocatalyst, oxide semiconductor coating materials may be a more suitable choice for QDs. For example, amorphous TiO₂ barriers and the dual-layers consisting of amorphous TiO₂ and Ni-oxide have been introduced as the powerful strategies to protect the photoelectrode [19–22].

* Corresponding author.

E-mail address: liangli117@sjtu.edu.cn (L. Li).

Actually, in the case of the CuInS₂/TiO₂ heterostructures, the electron transfer is favorable from CuInS₂ to TiO₂, while holes maintained in CuInS₂ QDs because of its higher valence band (VB) in comparison with TiO₂ [23]. In fact, the excess holes accumulated in VB of QDs could induce an acute photocorrosion, which led to the decreased photocatalytic performance [24]. Thus, the transfer of the holes from the VB of CuInS₂ QDs could be an effective approach to inhibit the photocorrosion. Besides the commonly used sacrificial agents of Na₂S and Na₂SO₃ for hole-removing in the QD-photocatalytic system, loading a hole-capture carrier (hole accepting ligands [25] or amorphous hole-cocatalyst) is also a competent technique to hinder the photoinduced corrosion of QDs. Recently, it was demonstrated that amorphous TiO₂ could act as hole-capture material to facilitate the hole transfer and afford a certain extent of stability enhancement when it introduced to GaAs [21], BiVO₄ [22], and AgBr [26] as cocatalyst, which gives an excellent hint for improving the stability of the QD-contained photocatalyst.

It has been reported that the nano-photocatalysts often present in powder form, which may exhibit superior performance at the beginning [27]. However, the amount of the photocatalysts would be inevitably reduced during the recycle process, since the powders are easy to be lost [28]. The other problem is the efficient separation and recycling of photocatalysts in practical utilization. Three-dimensional gel-based composites have aroused intensive interest recently [28,29]. The photocatalyst gel in a nanostructured bulk morphology could overcome the aforementioned problems and display as a convenient recyclable photocatalyst. Therefore, if we introduce Titanium (IV) isopropoxide to form a co-gelation with CIS/ZnS-TiO₂, the formed amorphous TiO₂ coatings cannot only facilitate the photocatalyst recycling, but also protect the CIS/ZnS QDs from photocorrosion.

On the basis of these considerations, in this work we have fabricated an efficient and stable solar light-driven photocatalyst, employing a co-gelation approach to prepare a bulk gel constructed by the CIS/ZnS-TiO₂ heterostructures embedded in the amorphous TiO₂ coatings. Photocatalytic reduction of Cr (VI) was selected to investigate the photocatalytic performance of the samples. The resultant CIS/ZnS-TiO₂ gel exhibited better resistance of photocorrosion and recycle performance in comparison with the uncoated CIS/ZnS-TiO₂. By studying the X-ray photoelectron spectroscopy (XPS) spectra of the powder and gel samples, the effect of the amorphous TiO₂ on the photostability of the CIS/ZnS-TiO₂ gel was elucidated. Amorphous TiO₂ coatings could not only serve as a physical protection layer, but also inhibit the photocorrosion of CIS/ZnS QDs through the rapid holes separation. The introduction of amorphous TiO₂ coatings along with the appearance of bulk gel realized efficient charge separation, drastically enhanced the stability, and facilitated the recycling of photocatalyst, which may be an attractive candidate for practical application. This work illuminates a new sight for the development of high photoactive and stable QDs-coupled photocatalysts.

2. Experimental methods

2.1. Materials

1-dodecanethiol (DDT, 98%), 1-octadecene (ODE, 90%), copper iodide (CuI, 99.95%), zinc acetate (Zn(Ac)₂, 99%), *n*-butylamine (99%), oleylamine (90%), TiO₂ (anatase, 25 nm), acetate (\geq 99.8%), and 3-mercaptopropionic acid (MPA, 98%) were purchased from Aladdin. Oleic acid (OA, 90%) was provided by Sigma-Aldrich. Indium acetate (In(Ac)₃, 99.99%) was obtained from Alfa Aesar. Titanium (IV) isopropoxide (TTIP, 98%) was obtained from J&K Scientific Ltd. All the chemicals were used without further purification.

2.2. Photocatalyst preparation

2.2.1. Preparation of CuInS₂ core QDs

CuInS₂ core QDs were prepared via a modified literature method. Typically, CuI (2.8 g), In(Ac)₃ (4.5 g), oleylamine (15 mL), DDT (145 mL), and ODE (145 mL) were mixed in a three-neck flask under magnetic stirring. The mixture was degassed at 120 °C for 1 h, then further heated to 230 °C under a nitrogen atmosphere. The reaction system was stayed at 230 °C for 40 min and then cooled to room temperature.

Zn(OA)₂ precursors (0.50 mmol mL⁻¹) were prepared as follows: Zn(Ac)₂ (32.11 g) was added into a three-neck flask containing OA (105 mL), ODE (210 mL), and *n*-butylamine (35 mL). The mixture was heated to 120 °C and refluxed for 30 min to form an optically transparent solution, then stored as a stock solution after cooling down to room temperature.

2.2.2. Preparation of CIS/ZnS QDs

Briefly, the CuInS₂ core solution (0.8 mmol, diluted to 40 mL with ODE) were added into a three-neck flask, and evacuated for 30 min at 120 °C under magnetic stirring. The reaction temperature was raised and maintained at 230 °C under a nitrogen atmosphere to allow the growth of ZnS shell. Zn(OA)₂ solution and an equi-volume amount of DDT were injected into the reaction vessel by syringes pump at a rate of 3.2 mL h⁻¹, respectively. The resulted QDs solution was cooled down to room temperature, purified several times by methanol and hexane, and then resuspended in toluene. On the basis of our previously work, the ZnS shell overcoating time was settled as 5 h with a shell thickness around 1.25 nm, which allowed the electron wave functions delocalization from core to the ZnS shell. And, the corresponding core/shell QDs was labeled as CIS/ZnS QDs in this work.

2.2.3. Formation of CIS/ZnS-TiO₂ nanocomposites

For the introduction of QDs to TiO₂ nanoparticles, the ligands of CIS/ZnS QDs were exchanged with MPA, which can act as the bifunctional linker. In the ligand exchange process, CIS/ZnS QDs (0.04 mmol) were dispersed in toluene and added to a methanol solution of MPA (36 μL) under stirring, and the solution was continuous stirring for 8 h to obtain the MPA-capped CIS/ZnS QDs. To form the CIS/ZnS-TiO₂ photocatalysts, anatase TiO₂ (20 mg) with an average size of 25 nm was chosen and subsequently mixed with precalculated amount of MPA-capped CIS/ZnS QDs solution through magnetic stirring for 4 h. Then, the obtained nanocomposites were rinsed with methanol to remove excess MPA. Finally, the CIS/ZnS-TiO₂ heterojunction photocatalyst was acquired by precipitation and dried at 50 °C in a vacuum drying oven. For the amorphous TiO₂ coating gel, the CIS/ZnS-TiO₂ nanocomposites were redispersed in anhydrous ethanol.

The sol-gel process was carried out to form amorphous TiO₂ gel matrix encapsulated CIS/ZnS-TiO₂ nanocomposites by using Titanium (IV) isopropoxide (TTIP) as the titania precursor. CIS/ZnS-TiO₂ nanocomposites were first dispersed in 1 mL of anhydrous ethanol, followed by the introduction of TTIP solution (185 μL TTIP diluted by 500 μL anhydrous ethanol). Three other different amounts of TTIP solution (0.25, 0.75, and 1 mmol) were introduced to the system to observe the effect of amorphous TiO₂ contents on photocatalytic activity. And the resulted solution was stirred at 25 °C for 30 min. After homogenizing, a catalyst solution (644 μL, anhydrous ethanol, acetic acid, and distilled water in volume ratio of 14:1:2) was slowly added to the above homogeneous solution under magnetic stirring in water bath at 40 °C. The mixture was stirred for 30 min and let it still till to the forming of wet gel. Following gelation, the vials contained the wet gel were sealed and allowed to age for 3 days at ambient temperature (ca. 25 °C). Afterwards, the

resulted wet gels were dried in a vacuum drying oven at 40 °C, 60 °C, and 80 °C separately for 2 h.

2.3. Characterization

Transmission electron microscopy (TEM) and High-resolution transmission electron microscopy (HRTEM) images were characterized using a JEM-2100F electron microscope. The surface morphologies of samples were obtained by Extreme-resolution analytical field emission (SEM, JEOL JSM-7800F Prime) at an accelerating voltage of 10.0 kV. The X-ray diffraction (XRD) patterns of samples were carried out on a Shimadzu XRD-6100 diffractometer using Cu radiation. Attenuated total reflectance infrared (ATR-IR) spectra were performed on a Thermo Nicolet 6700 spectrometer (USA). X-ray photoelectron spectroscopy (XPS) analysis was collected by a Kratos Axis Ultra-DLD spectrometer with a monochromatic Al K α radiation source ($\hbar\nu = 1486.6$ eV). Raman analysis was performed on Dispersive Raman Microscope (Senterra R200-L, Bruker Optics) with the 532 nm laser line. Ultraviolet visible (UV-vis) diffuse reflectance spectra (using BaSO₄ as the reference) and fluorescence emission of photocatalysts were recorded by a Perkin-Elmer Lambda 750 UV/VIS/NIR spectrometer and Ocean Optics LS-450, respectively.

2.4. Photocatalytic performance

The photocatalytic performance of the obtained samples was evaluated by the photocatalytic reduction of Cr (VI) under simulated solar light irradiation. Typically, the as-prepared photocatalyst was added into a vial containing 50 mL Cr (VI) aqueous solution (20 mg L⁻¹). AXe lamp (CEL-S500, Aulight, China) was used as the simulated solar light source with an optical power density of 90 mW cm⁻². No cut-off filter was employed. Prior to irradiation, the suspension was kept in the dark for 30 min to attain the adsorption/desorption equilibrium under ambient conditions. At certain time intervals, solution was sampled from the reaction mixture and analyzed by recording the absorbance at 350 nm using UV-vis spectroscopy. Note that the mixture solution using CIS/ZnS-TiO₂ powder as photocatalyst was centrifuged to remove the photocatalysts for measurement, while the solution sampled from the gel reaction vial can be monitored directly. For comparison, the reduction of Cr (VI) solution under irradiation without catalyst was also tested. Meanwhile, the reusability of the photocatalyst was also evaluated by the following procedure: the photocatalyst was washed with distilled water and acetone for several times after photocatalytic reduction and then retested in the fresh mixture solution of Cr (VI) under the same experimental conditions as mentioned above.

3. Results and discussion

3.1. XRD and morphology analysis

The crystallographic structures of the amorphous TiO₂ gel and the CIS/ZnS-TiO₂ gel with different CIS/ZnS QD contents (5%, 10%, 20%, and 30%) and were determined by XRD analysis and shown in Fig. 1a. The XRD patterns of the CIS/ZnS-TiO₂ gels indicated that the samples were well crystallized. The distinct diffraction peaks at 25.30°, 37.79°, 48.03°, 53.88°, and 55.05° matched well with the (101), (004), (200), (105), and (211) crystal planes of anatase TiO₂ (JCPDS 21-1272), respectively. The increased amount of CIS/ZnS QDs in the gels led to the enhanced diffraction peaks at 27.88°, 46.27°, and 55.06° corresponding to the reflection direction of CIS/ZnS QDs. Compared with pure CIS/ZnS-TiO₂ powder (Fig. S1), all the peaks can be indexed to the CIS/ZnS and TiO₂ phase, and the amorphous TiO₂ related peaks are not obviously appeared in the

CIS/ZnS-TiO₂ gels. Nevertheless, when we just check the XRD pattern of the amorphous TiO₂ gel alone, a broad peak around 25° is clearly present, which is attributed to the amorphous phase of TiO₂ derived from the hydrolysis of TTIP [30]. This demonstrated that the absence of the amorphous TiO₂-related peaks after the gel coating may arise from their amorphous structure with low crystallinity and the overlapping of the diffraction peaks of TiO₂ and CIS/ZnS QDs. The presence of amorphous TiO₂ could be further confirmed by the TEM images.

As shown in Fig. 1, the TEM images clearly illustrated an intuitive exhibition of morphologies for the obtained samples. Uniform CIS/ZnS QDs with a tetrahedral shape were utilized here and they mainly distributed in the range of 3.5–6.0 nm (Fig. S2). Fig. 1b demonstrated that the CIS/ZnS QDs were well dispersed on the TiO₂ nanoparticles, and their close contact resulted in the formation of CIS/ZnS-TiO₂ heterojunction, which is helpful for the fast interfacial electron transfer. Thus, the recombination of photogenerated electron-hole pairs is effectively reduced, and the photocatalytic activity can be accordingly enhanced [12]. This can be further confirmed by the high-resolution TEM (HRTEM) image (Fig. 1c). The observed lattice spacing of 0.314 nm in the tetrahedral QD is attributed to CIS/ZnS QDs, and the lattice spacing of 0.352 nm is assigned to the (101) plane of anatase TiO₂. For the CIS/ZnS-TiO₂ gel (20 wt% CIS/ZnS to TiO₂), the amorphous TiO₂ overlayer grew around CIS/ZnS-TiO₂ can be delineated (Fig. 1d), resulting in the encapsulation of CIS/ZnS-TiO₂ in the amorphous TiO₂ matrices. The lattice fringes of CIS/ZnS QDs and TiO₂ nanoparticles in the gels (Fig. 1e) exhibited more vagueness in comparison with the CIS/ZnS-TiO₂, which also certified the aforementioned concept. This is also observed in our previous study in the case of perovskites QDs embedding in silica spheres, where the lattice fringe of QDs was not easy to distinguish [31]. The amorphous TiO₂ may act as the protection coating material to enhance the stability and further reduce the combination of electron-hole pairs [32]. The morphological structures of the CIS/ZnS-TiO₂ gel were successively examined by scanning electron microscopy (SEM), as shown in Fig. 1f. The obtained CIS/ZnS-TiO₂ gel was mainly assembled of irregular-shaped grains in hundreds of nanometers with an internal microporous structure. Similar morphology can also be observed in other CIS/ZnS-TiO₂ gels with different proportion of CIS/ZnS QDs (Fig. S3).

3.2. FTIR, Raman, and XPS analysis

We used FTIR to examine the changes occurred in the samples after the introduction of amorphous TiO₂ coating (Fig. 2a). In comparison with CIS/ZnS QDs, a new peak at 1706 cm⁻¹ was assigned to C=O stretching vibration band [33], and the enhancing of asymmetric stretching vibration of –COOH [34] at 1556 cm⁻¹ clearly confirmed the existence of MPA on the surface of CIS/ZnS QDs. The typical Ti–O stretching mode in TiO₂ appeared as a wide peak around 600 cm⁻¹ [35]. Thus, the FTIR spectra likewise afforded evidence for the effectively combination of CIS/ZnS QDs and TiO₂. Nevertheless, the functional groups such as C–H (2918 cm⁻¹ asymmetric stretching vibration, 2849 cm⁻¹ symmetric stretching vibration) [36] and C=O (1706 cm⁻¹) of CIS/ZnS-TiO₂ were difficult to be distinguished in CIS/ZnS-TiO₂ gel. Such changes may somehow attribute to the emerging of CIS/ZnS-TiO₂ encapsulated in the amorphous TiO₂, which partly covered the surface features of CIS/ZnS-TiO₂. Notably, the formation of amorphous TiO₂ coating was further evidenced by the appearance of a new characteristic absorption peak around 710 cm⁻¹, which was generally corresponding to the Ti–O stretching mode of the amorphous structure titania [37]. Besides, a small peak at 1028 cm⁻¹ and a weak band around 3200 cm⁻¹ can be assigned to Ti–O–H [38,39], respectively, indicating the successful generation of amorphous TiO₂

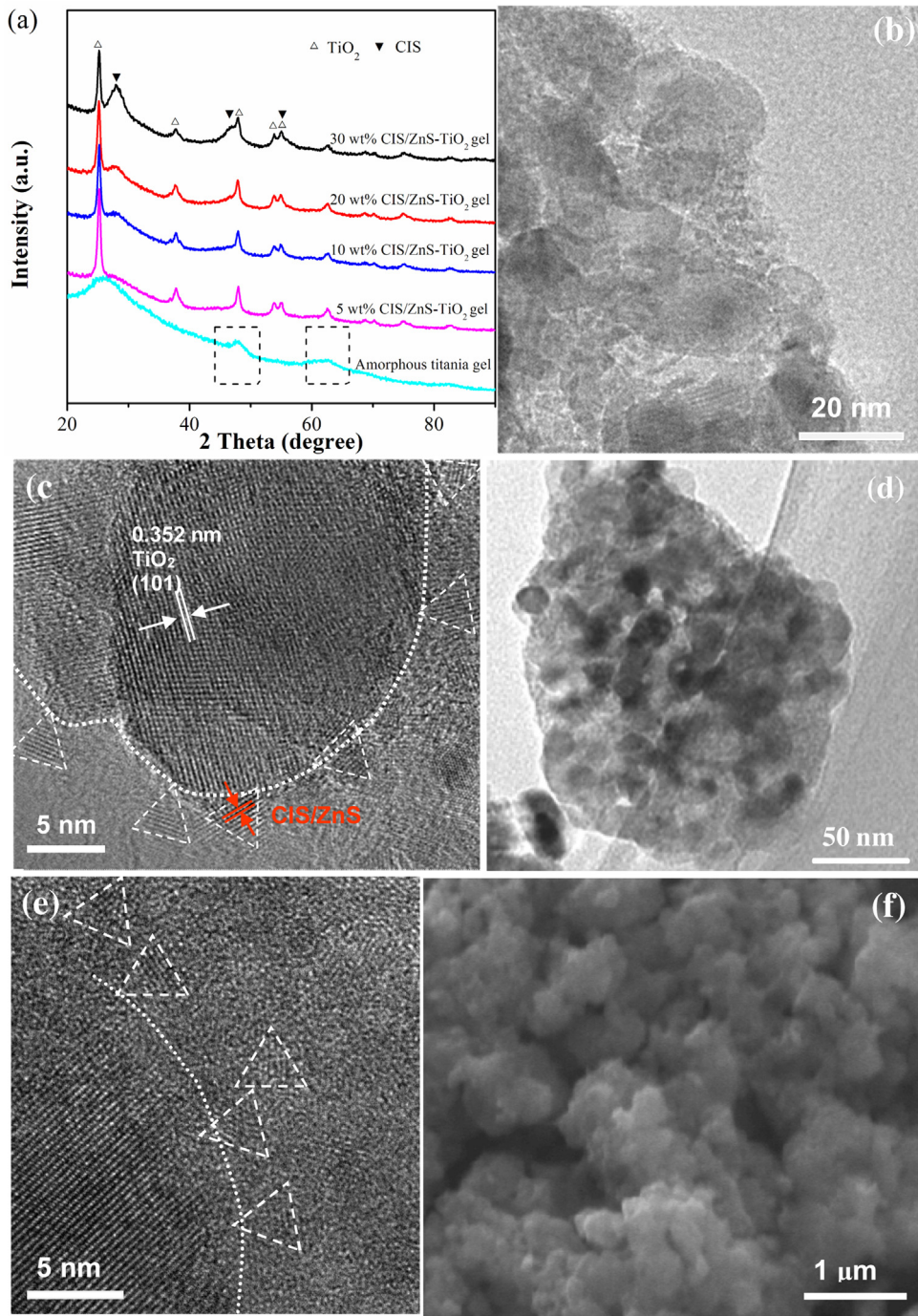


Fig. 1. (a) XRD patterns of CIS/ZnS-TiO₂ gel with different weight ratio of CIS/ZnS QDs. TEM and the corresponding HRTEM images of CIS/ZnS-TiO₂ (b, c) and CIS/ZnS-TiO₂ gel (d, e). (f) SEM images of CIS/ZnS-TiO₂ gel (20 wt% CIS/ZnS to TiO₂).

protection coating. Consequently, it is believed that the amorphous TiO₂ gel embedded with CIS/ZnS-TiO₂ was successfully obtained and would possess prominent activity and stability for photocatalysis. As shown in Fig. S4, the broad Raman spectrum and its relatively low intensity indicated that the prepared amorphous TiO₂ should be predominant in an amorphous structure with minor amounts related to anatase phase [40]. In addition, XPS spectra were also performed (Figs. 2 b and S5). The XPS spectra of CIS/ZnS-TiO₂ gel (Cu, In, Zn, S, C, and O) showed no obvious shift in comparison with that of CIS/ZnS-TiO₂ (Fig. S5), indicating that the state of the elements was not obviously affected by the integration of amorphous TiO₂ coating. The Ti 2p_{1/2} and Ti 2p_{3/2} of the CIS/ZnS-TiO₂ gel cen-

tered at 458.4 eV and 464.0 eV were attributed to the Ti⁴⁺ state [26]. A weak peak at 456.2 eV was distinguishable in the Ti 2p spectrum, which is due to the existence of Ti³⁺ states (i.e., O-vacancies) [41] in amorphous TiO₂ coating.

3.3. Optical absorption

The optical properties of as-prepared samples were investigated by UV-vis diffuse reflectance spectroscopy (DRS), as shown in Figs. S6 and 3. The CIS/ZnS-TiO₂ gel exhibited an intense and broad absorption in the visible light region compared with the pure TiO₂ gel. The existence of oxygen vacancies in amorphous TiO₂ extended

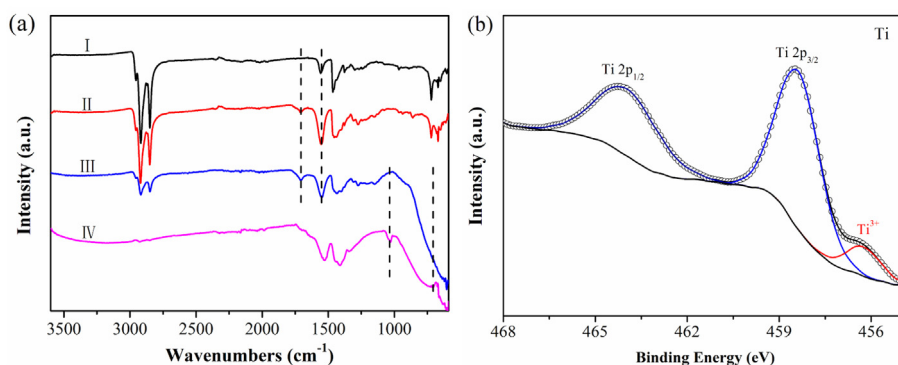


Fig. 2. (a) FTIR spectra of (I) CIS/ZnS QDs, (II) CIS/ZnS QDs after ligand exchange with MPA, (III) CIS/ZnS-TiO₂, and (IV) CIS/ZnS-TiO₂ gel; (b) Ti 2p XPS spectra of CIS/ZnS-TiO₂ gel.

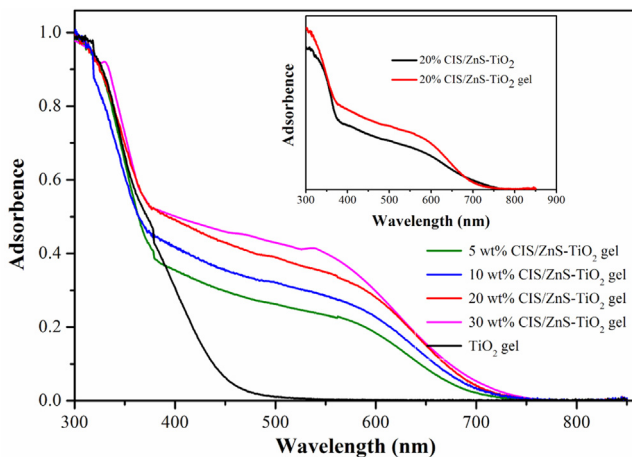


Fig. 3. UV-vis diffuse reflectance spectra of TiO₂ gel and CIS/ZnS-TiO₂ gel with different contents of CIS/ZnS QDs. The inset figure shows the UV-vis DRS comparison of CIS/ZnS-TiO₂ heterojunction photocatalyst and CIS/ZnS-TiO₂ gel.

the absorption of amorphous TiO₂ with an edge beyond 400 nm. Increase of CIS/ZnS QDs resulted in the absorption range shifted to longer wavelengths about 750 nm, which suggested an extended solar energy-harvesting capability and allowed the promotion of photocatalytic performance. The light absorption variation was well consistent with the amount of CIS/ZnS QDs content. As the increase of CIS/ZnS the light absorption of CIS/ZnS-TiO₂ exhibited an increase trend in the range of 400–750 nm. A change in the absorption of CIS/ZnS-TiO₂ gel was observed in comparison with the CIS/ZnS-TiO₂ powder (inset figure of Fig. 3), which is attributed to the beneficial affection of amorphous TiO₂ coatings arose from the scattering and multiple reflections of incident light within the amorphous TiO₂ coatings.

3.4. Photoluminescence properties

We also measured the photoluminescence (PL) intensity of the obtained samples to further explore the role of amorphous TiO₂ matrix, which could reveal the occurrence of charge transfer between QDs and TiO₂ [42]. The PL spectra of our CIS/ZnS QDs, CIS/ZnS-TiO₂, and CIS/ZnS-TiO₂ gel measured with an excitation wavelength of 470 nm were shown in Fig. 4a. The PL emission of CIS/ZnS QDs showed a significant quenching by the combination with TiO₂ nanoparticles. Notably, the PL intensity of CIS/ZnS-TiO₂ gel was obviously further decreased and exhibited the lowest PL signal after the introduction of amorphous TiO₂ matrix. This observation allowed us to prove the suppression of the electron-hole recombination, leading to the efficient spatial separation of

electron-hole. Moreover, we observed that the integration of amorphous TiO₂ resulted in enhanced electron-hole transfer, which would boost the photoatalytic reaction.

Further performed time-resolved PL measurement gave more insights into the charge separation, and the corresponding spectra of samples were shown in Fig. 4b. Note that the irradiation for time-resolved PL measurement allowed the excitation of CIS/ZnS QDs in this composite system since TiO₂ nanoparticles have no obvious absorption in visible range (460 nm) and cannot be directly excited. Notable changes of lifetimes occurred in CIS/ZnS-TiO₂ and the CIS/ZnS-TiO₂ gel sample in comparison with CIS/ZnS QDs as reference. The three curves can be well-fitted by exponential function, and the lifetimes were calculated to be 315 ns, 206 ns, and 115 ns for CIS/ZnS QDs, CIS/ZnS-TiO₂, and CIS/ZnS-TiO₂ gel, respectively. The decrease in lifetime may be attributed to couple of CIS/ZnS and TiO₂ nanoparticles, thus promotes carriers on the surface of QD transfer to TiO₂. After the introduction of amorphous TiO₂, it was possible to obtain more interface areas between CIS/ZnS QDs and TiO₂, and achieved a much shorter average lifetime and more effective separation probability of electron-hole pairs. Thus, integration of CIS/ZnS QDs with TiO₂ facilitated the efficient charge separation, and CIS/ZnS-TiO₂ gel in virtue of the succeeded amorphous TiO₂ encapsulation successfully realized further suppression of electron-hole recombination. This may lead to an enhancement of photocatalytic efficiency, which was in good agreement with the above PL results.

3.5. Photocatalytic performance and mechanism discussion

The performances of samples were evaluated by monitoring the photocatalytic reduction of Cr (VI) under simulated solar light irradiation. According to the photocatalytic activity of prepared CIS/ZnS-TiO₂ gel with different amorphous TiO₂ contents, when the addition amount of amorphous TiO₂ precursor (TTIP) was about 0.5 mmol, the resultant CIS/ZnS-TiO₂ gel exhibited the highest photocatalytic reduction efficiency of Cr (VI). Therefore, in this study, the addition amount of amorphous TiO₂ precursor was controlled. After irradiation for 2 h, the maximum reduction rate of Cr (VI) can be up to 98.95% over CIS/ZnS-TiO₂ gel (20 wt% CIS/ZnS to TiO₂), exhibiting evidently improved photocatalytic activity in comparison with the TiO₂ gel and CIS/ZnS gel. Individual TiO₂ gel and CIS/ZnS gel presented a reduction rate of 19.3% and 56.6%, respectively (Fig. 5a). When CIS/ZnS QDs was introduced to TiO₂, the reduction rate of CIS/ZnS-TiO₂ gel was increased depending on the proportion of CIS/ZnS in the composites, and a downturn appeared after an optimum CIS/ZnS content of 20%, which was similar to that of the CIS/ZnS-TiO₂ samples (Fig. S7a and b). The reduction efficiencies of Cr (VI) increased from 87.35% to 98.95% as the proportion of CIS/ZnS QDs from 5 wt% to 20 wt%, and decreased to

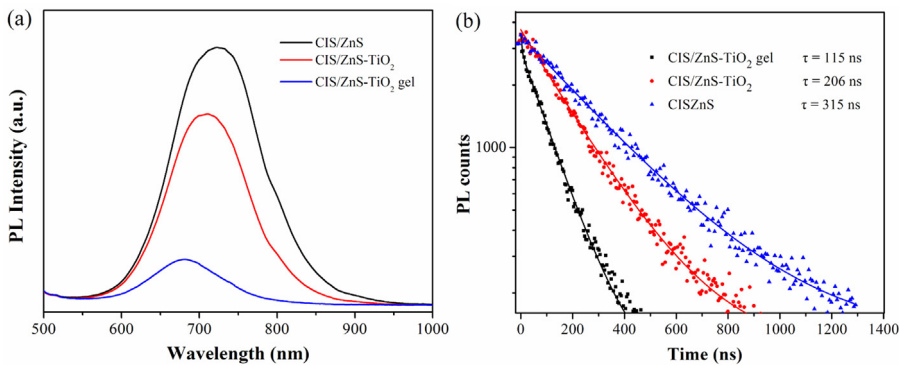


Fig. 4. (a) PL spectra of the blank CIS/ZnS QDs, CIS/ZnS-TiO₂, and CIS/ZnS-TiO₂ gel (20 wt% CIS/ZnS to TiO₂) powders. Excitation was at 470 nm. (b) The time-resolved PL decay spectra and fitting curves of the blank CIS/ZnS QDs, CIS/ZnS-TiO₂, and CIS/ZnS-TiO₂ gel powders detected at their corresponding steady state PL peak wavelengths with excitation of 460 nm.

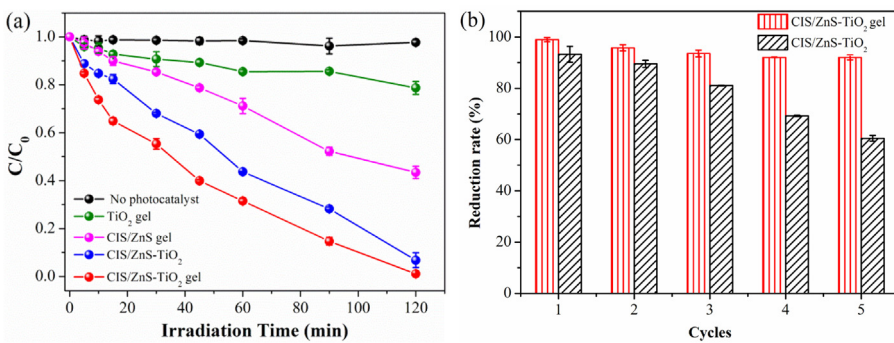


Fig. 5. (a) Photocatalytic reductive curves of Cr(IV) by as-prepared samples under simulated solar light. (b) Cycling photo-reduction of Cr(IV) by CIS/ZnS-TiO₂ and CIS/ZnS-TiO₂ gel (20 wt% CIS/ZnS to TiO₂) in comparison. Experiment conditions: optical power density 90 mW cm⁻², irradiation time of each cycle 2 h.

91.70% when the CIS/ZnS QD contents up to 30 wt%. These results indicated that the amount of CIS/ZnS QDs plays an important role for the photocatalytic reduction of Cr(IV). The excessive introduction of CIS/ZnS QDs might increase the chance of recombination of electrons and holes, resulting in the decrease of photocatalytic performance [14]. This phenomenon was also found in the case of photoelectrodes [12]. Additionally, compared with the CIS/ZnS-TiO₂ sample, the introduction of amorphous TiO₂ enhanced the photocatalytic reduction ability of CIS/ZnS-TiO₂ gel in virtue of the suppressed electron-hole recombination and improved solar light absorption, which were verified by the UV-vis spectra and time-resolved PL results.

Formation a promising photocatalyst would require the wonderful photostability, which was critical in practical application. The cycling experiments of Cr(IV) reduction by CIS/ZnS-TiO₂ and CIS/ZnS-TiO₂ gel (20 wt% CIS/ZnS to TiO₂) were determined, which exhibited the recyclability and photocatalytic stability (Fig. 5b). We can see that the photocatalytic activity of the CIS/ZnS-TiO₂ without amorphous TiO₂ coating drastically dropped to 65% of its initial value. The poor tolerance under solar light irradiation combined with the quality loss in recycles definitely accounted for its decrease of photocatalytic activity. The measured content of CIS/ZnS-TiO₂ was dropped to be about 85% of its original weight after the whole cycling process, while only approximately 3.55% quality loss can be found for bulk CIS/ZnS-TiO₂ gel. The CIS/ZnS-TiO₂ gel exhibited a high photocatalytic stability without noticeable decrease of performance during five cycles under applied condition, suggesting that it can be a promising potential method for photocatalyst to improve stability and facility-applications.

XPS analysis was used to obtain insights into the changes of CIS/ZnS-TiO₂ and CIS/ZnS-TiO₂ gel after five photocatalytic cycles (Fig. 6), which had an impact on the photocatalytic performance.

Herein, the S 2p band at 162.30 eV should be attributed to S from CIS/ZnS QDs [10]. Comparison of S 2p spectra before and after photocatalytic stability testing revealed no significant changes (a slight peak shift to 162.50 eV) for CIS/ZnS-TiO₂ gel. In contrary, obvious differences were observed for CIS/ZnS-TiO₂. Accompanying by the band shift to higher binding energy (162.81 eV), a new peak emerged at 168.80 eV, which suggested the formation of SO₄²⁻-oxygenated form of CIS/ZnS QDs [43]. This suggested that the amorphous TiO₂ acted as an effective protection coating (i.e. physically protection or/and efficient diversion of photogenerated holes from CIS/ZnS QDs) and enhanced the photostability of CIS/ZnS QDs for photocatalysis, similar to previous studies for photoanode [41]. Such chemical changes somehow accounted for the different photocatalytic performance of CIS/ZnS-TiO₂ and CIS/ZnS-TiO₂ gel over cycling tests. Meanwhile, analysis of Cr 2p spectra confirmed the existence of Cr. The Cr 2p_{3/2} peak centered at 576.53 eV could be attributed to Cr(III) in Cr₂O₃ [44], which may result from the photocatalytic reduction of adsorbed Cr(IV) ions. Nevertheless, the XPS Cr 2p_{3/2} spectra region of CIS/ZnS-TiO₂ powder can be deconvoluted into two different peaks at 576.53 eV and 579.09 eV, respectively. The peak at 579.09 eV revealed the subsistence of Cr(IV) [44], which generated from the decreased photocatalytic activity of CIS/ZnS-TiO₂ after its cycling tests, leaving partial adsorbed Cr(IV) ions out of reduction. In this case, the amorphous TiO₂ matrix in CIS/ZnS-TiO₂ gel not only provided an enhanced photocatalytic activity, but also could protect the CIS/ZnS QDs from photocorrosion and maintain its excellent performance.

Upon the simulated solar-light irradiation, CIS/ZnS QDs could be excited by visible-light irradiation and UV-light excited the TiO₂ nanoparticles. For TiO₂-coupled CIS/ZnS nanocomposites, the band alignments facilitated the transport of photogenerated electrons from CIS/ZnS QDs to TiO₂ nanoparticles [10], enabling the separa-

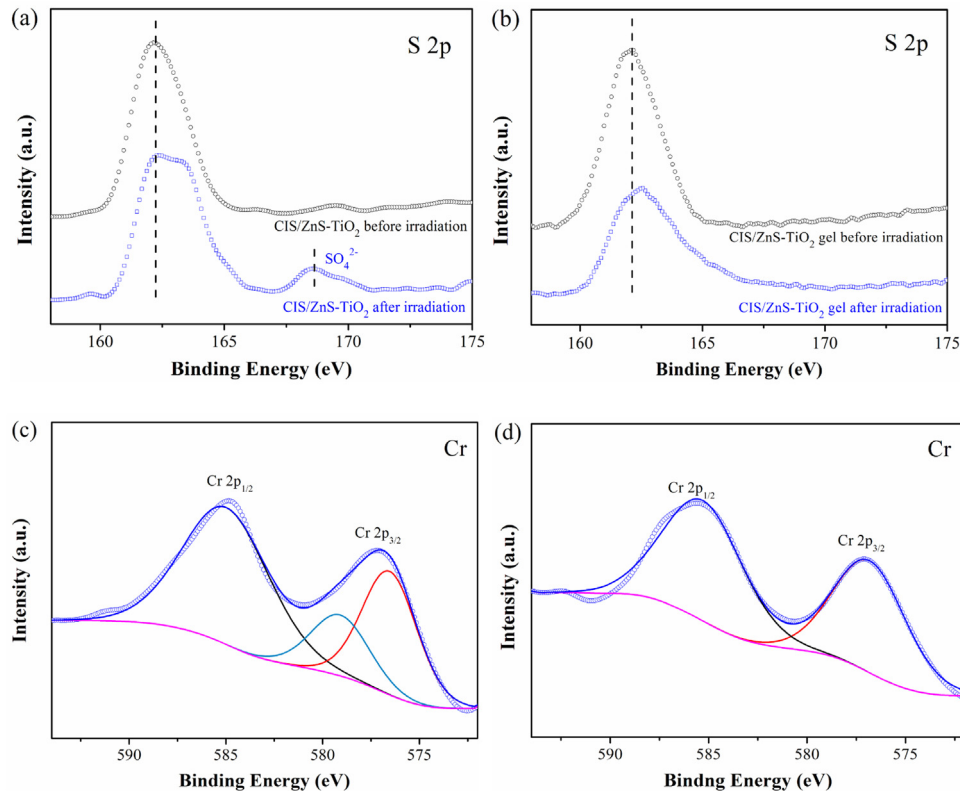


Fig. 6. S 2p XPS spectra of (a) CIS/ZnS-TiO₂ and (b) CIS/ZnS-TiO₂ gel before and after photocatalytic reaction; Cr 2p XPS spectra of (c) CIS/ZnS-TiO₂ and (d) CIS/ZnS-TiO₂ gel after photocatalytic reaction.

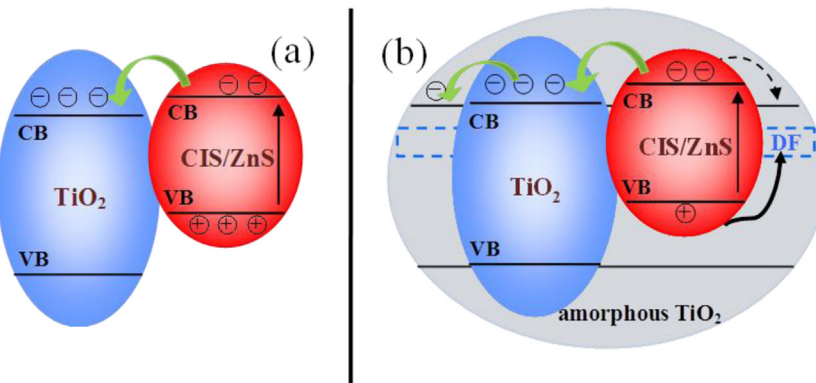


Fig. 7. Schematic illustration of photogenerated electron-hole separation over the CIS/ZnS-TiO₂ photocatalysis (a) without and (b) with amorphous TiO₂ coatings. CB, conduction band; VB, valence band; DF, defect states.

tion of photogenerated electron-hole pairs and successively leading to an improved photocatalytic activity. However, the deeper VB of crystalline TiO₂ (in this case, anatase TiO₂) blocked the transfer of holes from CIS/ZnS VB. Thus, the holes were retained in the CIS/ZnS QDs and photocorrosion occurred under photo-excitation without sacrificial agent [24], consequently resulting in a suppressed photocatalytic performance. As for the CIS/ZnS-TiO₂ gel with CIS/ZnS-TiO₂ heterostructures encapsulated in amorphous TiO₂ matrix, the possible band diagram under simulated-solar light irradiation is shown in Fig. 7. Given the noncontinuous cover or contact of CIS/ZnS with TiO₂ in CIS/ZnS-TiO₂ nanocomposites, the integration of CIS/ZnS-TiO₂ with amorphous TiO₂ coatings warranted the further effective migration of interfacial electrons and enhanced inhibition of recombination for photogenerated electron-hole. Unlike the blocking of hole transport in anatase TiO₂, the valance band holes of CIS/ZnS QDs could be transferred with

the assistance of defect states in chemically stable amorphous TiO₂ coatings [21,41]. The defect associated with the introduction of amorphous TiO₂ was supported by aforementioned XPS results (Fig. 2b). The facilitate capture of holes from VB of CIS/ZnS may avoid the holes accumulation on CIS/ZnS QDs and acquire certain inhibition of photocorrosion. A certain extent crystallization of amorphous TiO₂ coatings, as reflected by the XRD measurements, accounted for the transport of electrons. Besides, the amorphous TiO₂ may cause recombination of electron-hole, which should not be the dominant process in this case. Considering the actual photocatalytic activity results, we can see that the benefits of TiO₂ protection coatings overweighted the undesirable electron-hole recombination. Additionally, the amorphous TiO₂ could function as a physical protection layer to barrier the permeation of oxygen. Consequently, the existence of amorphous TiO₂ matrix worked as physical barrier while facilitated the migration of holes from VB

of CIS/ZnS QDs provided synergistic contributions to the enhanced photostability.

4. Conclusions

In summary, we have demonstrated a facile sol-gel method to encapsulated CIS/ZnS-TiO₂ nanocomposites in amorphous TiO₂ matrix, and the resultant CIS/ZnS-TiO₂ gel possessed an excellent photocatalytic activity for reduction of Cr (VI) and obviously enhanced photostability under the simulated solar-light irradiation. The incorporation of amorphous TiO₂ coatings in our designed photocatalyst accounted for the remarkable photocatalytic behavior via benefiting its solar-light absorption, photogenerated electron-hole separation, and corrosion resistance. Actually, distinctive heterojunction coupling and band alignment of CIS/ZnS-TiO₂ gel derived the enhancement of photogenerated electron-hole separation in comparison with CIS/ZnS-TiO₂ nanocomposites, demonstrated by the PL spectra and time-resolved PL measurement. The TiO₂ coating could work as a protecting layer to isolate the CIS/ZnS QDs from surrounding oxygen. Furthermore, the allocation of defect states in amorphous TiO₂ layer offered the opportunity to capture and consume holes from CIS/ZnS QDs, and subsequently overcame the photocorrosion induced by photogenerated holes. The current study successfully explored the employment of amorphous TiO₂ gel matrix in protecting unstable CIS/ZnS QDs and cycling stability. It is expected to open a logical extension to fabricate other chalcogenide semiconductors-based stable photocatalyst for efficient solar light utilization.

Acknowledgements

This work was supported by the National Natural Science Foundation of China (NSFC 21271179, 51278294, and 21607101), Program for New Century Excellent Talents (NCET-13-0364), the National High Technology Research and Development Program (No. 2012AA062504), and China Postdoctoral Science Foundation (2016M590363).

Appendix A. Supplementary data

Supplementary data associated with this article can be found, in the online version, at <http://dx.doi.org/10.1016/j.apcatb.2016.11.055>.

References

- [1] X. Yu, A. Shavel, X. An, Z. Luo, M. Ibáñez, A. Cabot, J. Am. Chem. Soc. 136 (2014) 9236–9239.
- [2] A. Fujishima, K. Honda, Nature 238 (1972) 37–38.
- [3] W.T. Sun, Y. Yu, H.Y. Pan, X.F. Gao, Q. Chen, L.M. Peng, J. Am. Chem. Soc. 130 (2008) 1124–1125.
- [4] Y. Hu, X.H. Gao, L. Yu, Y.R. Wang, J.Q. Ning, S.J. Xu, X.W.D. Lou, Angew. Chem. Int. Ed. 52 (2013) 5636–5639.

- [5] H.N. Kim, T.W. Kim, I.Y. Kim, S.J. Hwang, Adv. Funct. Mater. 21 (2011) 3111–3118.
- [6] Y.Q. Shi, K.Q. Zhou, B.B. Wang, S.H. Jiang, X.D. Qian, Z. Gui, R.K.K. Yuen, Y. Hu, J. Mater. Chem. A 2 (2014) 535–544.
- [7] C. Harris, P.V. Kamat, ACS Nano 3 (2009) 682–690.
- [8] K.P. Acharya, T.R. Alabi, N. Schmall, N.N. Hewa-Kasakarage, M. Kirsanova, A. Nemchinov, E. Khon, M. Zamkov, J. Phys. Chem. C 113 (2009) 19531–19535.
- [9] C. Wang, R.L. Thompson, P. Ohodnicki, J. Baltrus, C. Matranga, J. Mater. Chem. 21 (2011) 13452–13457.
- [10] T. Li, X. Li, Q. Zhao, Y. Shi, W. Teng, Appl. Catal. B: Environ. 156 (2014) 362–370.
- [11] F. Shen, W. Que, Y. Liao, X. Yin, Ind. Eng. Chem. Res. 50 (2011) 9131–9137.
- [12] I. Tsuji, H. Kato, A. Kudo, Chem. Mater. 18 (2006) 1969–1975.
- [13] S.T. Selvan, T.T. Tan, J.Y. Ying, Adv. Mater. 17 (2005) 1620–1625.
- [14] S. Jun, J. Lee, E. Jang, ACS Nano 7 (2013) 1472–1477.
- [15] P.H. Rao, W. Yao, Z.C. Li, L. Kong, W.Q. Zhang, L. Li, Chem. Commun. 51 (2015) 8757–8760.
- [16] Z.C. Li, W. Yao, L. Kong, Y.X. Zhao, L. Li, J. Am. Chem. Soc. 137 (2015) 12430–12433.
- [17] L.L. Yan, Z.C. Li, M.X. Sun, G.Q. Shen, L. Li, ACS Appl. Mater. Interfaces 31 (2016) 20048–20056.
- [18] W. Kim, T. Tachikawa, T. Majima, W. Choi, J. Phys. Chem. C 113 (2009) 10603–10609.
- [19] J. Gu, Y. Yan, J.L. Young, K.X. Steirer, N.R. Neale, J.A. Turner, Nat. Mater. 15 (2016) 456–460.
- [20] M.T. McDowell, M.F. Lichterman, J.M. Spurgeon, S. Hu, I.D. Sharp, B.S. Brunschwig, N.S. Lewis, J. Phys. Chem. C 118 (2014) 19618–19624.
- [21] S. Hu, M.R. Shaner, J.A. Beardslee, M. Lichterman, B.S. Brunschwig, N.S. Lewis, Science 344 (2014) 1005–1009.
- [22] D. Eisenberg, H.S. Ahn, A.J. Bard, J. Am. Chem. Soc. 136 (2014) 14011–14014.
- [23] R. Marschall, Adv. Funct. Mater. 24 (2014) 2421–2440.
- [24] H.G. Yu, X. Huang, P. Wang, J.G. Yu, J. Phys. Chem. C 120 (2016) 3722–3730.
- [25] I.S. Liu, H.H. Lo, C.T. Chien, Y.Y. Lin, C.W. Chen, Y.F. Chen, W.F. Su, S.C. Liouc, J. Mater. Chem. 18 (2008) 675–682.
- [26] H.G. Yu, W.Y. Chen, X.F. Wang, Y. Xu, J.G. Yu, Appl. Catal. B: Environ. 187 (2016) 163–170.
- [27] M. Zhu, P. Chen, M. Liu, ACS Nano 5 (2011) 4529–4536.
- [28] Y. Fan, W. Ma, D. Han, S. Gan, X. Dong, L. Niu, Adv. Mater. 27 (2015) 3767–3773.
- [29] B. Qiu, M. Xing, J. Zhang, J. Am. Chem. Soc. 136 (2014) 5852–5855.
- [30] D.S. Zhang, T. Yoshida, T. Oekermann, K. Furuta, H. Minoura, Adv. Funct. Mater. 16 (2006) 1228–1234.
- [31] S.Q. Huang, Z.C. Li, L. Kong, N.W. Zhu, A.D. Shan, L. Li, J. Am. Chem. Soc. 138 (2016) 5749–5752.
- [32] J.S. Luo, S.D. Tilley, L. Steier, M. Schreier, M.T. Mayer, H.J. Fan, M. Gratze, Nano Lett. 15 (2015) 1395–1402.
- [33] L. Etgar, T. Moehl, S. Gabriel, S.G. Hickey, A. Eychmüller, M. Gratzel, ACS Nano 6 (2012) 3092–3099.
- [34] M. Misra, S. Singh, A.K. Paul, M.L. Singla, J. Mater. Chem. C 3 (2015) 6086–6093.
- [35] S.D. Perera, R.G. Mariano, K. Vu, N. Nour, O. Seitz, Y. Chabal, K.J. Balkus Jr., ACS Catal. 2 (2012) 949–956.
- [36] X.C. Jiang, T. Herricks, Y.N. Xia, Adv. Mater. 15 (2003) 1205–1209.
- [37] S. Liu, S. Pang, H. Huang, X. Su, Analyst 139 (2014) 5852–5857.
- [38] Y. Xie, X. Liu, A. Huang, C. Ding, P.K. Chu, Biomaterials 26 (2005) 6129–6135.
- [39] K.L. Ding, Z.J. Miao, Z.M. Liu, Z.F. Zhang, B.X. Han, G.M. An, S.D. Miao, Y. Xie, J. Am. Chem. Soc. 129 (2007) 6362–6363.
- [40] C. Liang, K. Terabe, T. Hasegawa, M. Aono, Appl. Phys. Express 1 (2008) 064002.
- [41] J. Qiu, G.T. Zeng, M.A. Ha, M.Y. Ge, Y.J. Lin, M. Hettick, B.Y. Hou, A.N. Alexandrova, A. Javey, S.B. Cronin, Nano Lett. 15 (2015) 6177–6181.
- [42] J.B. You, L. Meng, T.B. Song, T.F. Guo, Y.M. Yang, W.H. Chang, Z.R. Hong, H.J. Chen, H.P. Zhou, Q. Chen, Y.S. Liu, N.D. Marco, Y. Yang, Nat. Nanotechnol. 11 (2016) 75–81.
- [43] B.H. Yang, P.H. Holloway, Adv. Funct. Mater. 14 (2004) 152–156.
- [44] L. Dupont, E. Guillou, Environ. Sci. Technol. 37 (2003) 4235–4241.